Optoacoustic Cooling of Traveling Hypersound Waves

Laura Blázquez Martínez,* Philipp Wiedemann,* Changlong Zhu,* Andreas Geilen, and Birgit Stiller†
Max Planck Institute for the Science of Light, Staudtstr. 2, 91058, Erlangen, Germany
and Department of Physics, Friedrich-Alexander Universität Erlangen-Nürnberg, Staudtstr. 7, 91058 Erlangen, Germany

(Received 31 May 2023; revised 6 November 2023; accepted 27 November 2023; published 11 January 2024)

We experimentally demonstrate optoacoustic cooling via stimulated Brillouin-Mandelstam scattering in a 50 cm long tapered photonic crystal fiber. For a 7.38 GHz acoustic mode, a cooling rate of 219 K from room temperature has been achieved. As anti-Stokes and Stokes Brillouin processes naturally break the symmetry of phonon cooling and heating, resolved sideband schemes are not necessary. The experiments pave the way to explore the classical to quantum transition for macroscopic objects and could enable new quantum technologies in terms of storage and repeater schemes.

DOI: 10.1103/PhysRevLett.132.023603

Introduction.—Cooling mechanical vibrations to the quantum ground state has recently been achieved in diverse optomechanical cavity configurations, such as micromechanical bulk resonators [1], drums embedded in superconducting microwave circuits [2], silicon optomechanical nanocavities [3], levitated nanoparticles [4], or bulk acoustic wave resonators [5]. The experimental approaches used so far to achieve this state start with the system at cryogenic temperatures, in the mK regime inside a dilution refrigerator, decreasing the thermal population of phonons severely. Nonetheless, reaching the quantum ground state has been made possible only by the use of additional laser-based techniques, such as coupling to highly dampened solid state systems [6,7], feedback cooling [8–11], or resolved sideband cooling [12–17]. The latter, also known as dynamical backaction, is based on the engineering of both cavity resonances and laser pump frequencies to favor the cooling over the heating process of a given phonon mode.

Reaching the quantum ground state is often a prerequisite for the study of quantum phenomena and enables applications in precision metrology [18,19], phonon thermometry [20,21], quantum state generation [22–24], or tests of fundamental physics [25,26]. So far, however, the research focus was on optomechanical cavity structures, in which distinct mechanical resonances (standing density waves), interact with specific optical frequencies, thus providing efficient coupling. Despite this fact, a process bound to narrow mechanical resonances limits both the bandwidth of the optomechanical interaction and its application to parallel multifrequency quantum operations.

An alternative approach is pursued by waveguide optomechanics, in which light can interact with traveling acoustic waves. The optical waves, which can be transmitted at any wavelength in the transparency window of the material, usually interact with a broad continuum of acoustic phonons. This strong interaction is enabled by electrostriction, radiation pressure, and photoelasticity, the physical phenomena behind stimulated Brillouin-Mandelstam scattering (SBS) [27]. SBS has received great interest for its broad range of applications in optical fibers or integrated photonic waveguides, such as sensing [28–30], signal processing [31–33], light storage [34–36], integrated microwave photonics [37–39], and lasing [40–42]. The viable application of SBS for active cooling in waveguides has been theoretically proposed [43,44]. First experimental results show cooling via SBS in optomechanical cavities [45] and integrated silicon waveguides [46], with cooling rates in the order of tens of Kelvin. Nonetheless, for continuous systems such as waveguides, achieving high SBS cooling rates remains an open challenge. So far, no experimental platform has shown the combination of Brillouin gain and acoustic dissipation rate that allows cooling to the quantum ground state [43,46,47].

Here, we experimentally demonstrate optoacoustic cooling of a band of continuous traveling acoustic waves in a waveguide system at room temperature. Without using a cryogenic environment, the acoustic phonons at 7.38 GHz are cooled by 219 K, reaching an effective mode temperature of 74 K. The cooled acoustic waves extend over a macroscopic length of 50 cm in a tapered chalcogenide glass photonic crystal fiber (PCF). The asymmetry of anti-Stokes and Stokes processes in the considered backward SBS interaction provides natural symmetry breaking in the heating-cooling of phonons and therefore no sideband cooling is necessary. We underpin our experimental results with a theoretical model that reproduces the replenishing of acoustic phonons by dissipation in a strong Brillouin-Mandelstam cooling regime. Given the long interaction length of 50 cm, the mechanical object addressed in the interaction is more massive than standard microresonators. Achieving ground state cooling of such a macroscopic phonon would pave the way toward exploring the transition of classical to quantum physics.

Experimental setup.—The setup used for the experiment is shown in Fig. 1(a). The output of a continuous wave (CW) laser at wavelength $\lambda_p = 1550$ nm is divided in two branches, pump and local oscillator (LO). The pump light is modulated into 100 ns long square pulses, with 25% duty cycle, amplified via an erbium-doped fiber amplifier (EDFA) and filtered with a band-pass filter (BPF). The fixed output of the EDFA can be controlled via a variable attenuator, allowing one to study the SBS resonances as a function of pump power. The coupling into the sample, a tapered chalcogenide glass solid core single mode PCF from Selenoptics, is done via free space. The glass composition is $Ge_{10}As_{22}Se_{68}$, with a SBS resonance of $\Omega_B/2\pi(1550\text{ nm}) = 7.38$ GHz. The PCF air-filling ratio is 0.48 [Fig. 1(b)] and the insertion and transmission loss through the fiber is -3.64 dB in total. The initial core diameter is 12 μm, which is tapered down to 3 μm at the waist, with a length of 50 cm [Fig. 1(c)]. An infrared (IR)

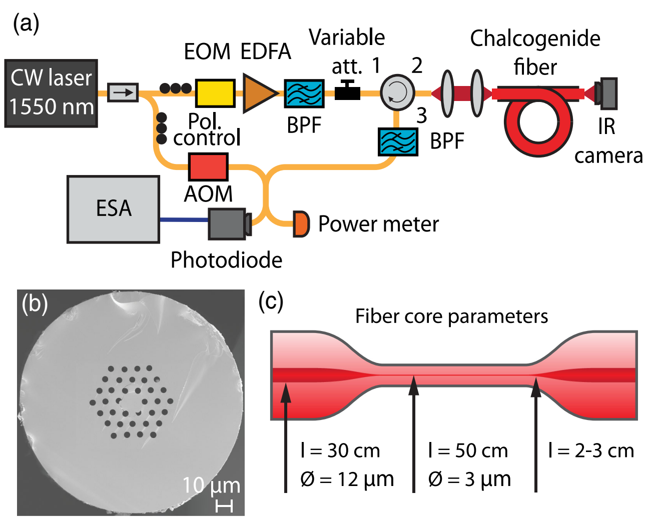

FIG. 1. (a) Diagram of the experimental setup used for the measurement of the backscattered SBS signal as a function of input power via heterodyne detection. CW: continuous wave; EOM (AOM): electro-optical (acousto-optical) modulator; EDFA: erbium-doped fiber amplifier; BPF: band-pass filter; ESA: electrical spectrum analyzer. (b) Scanning electron microscope image of the cross section of the untapered chacogenide glass PCF. The air-filling ratio of this fiber is 0.48 and it has a core diameter of 12 μm. (c) Diagram of the tapered sample. The taper waist has a length (l) of 50 cm and a core diameter of 3 μm. The waist is connected to 30 cm sections of untapered fiber, one on each side, via transitions of 2–3 cm in length.

camera allows one to visualize the optical mode propagating through the core and optimize coupling. As the SBS signal is backscattered, a circulator stops it from going back into the laser, redirecting it into the detection part of the setup. Given the high Fresnel coefficients of the fiber facets, another BPF is used to filter out the strong elastic pump back-reflection. The filtered signal is mixed with a frequency-shifted LO, via a 200 MHz acousto-optic modulator (AOM), to perform heterodyne detection. The resulting optical interference is detected with a photodiode and the transduced electrical signal measured with an electrical spectrum analyzer (ESA). The experiment is performed at room temperature (293 K).

Experimental results.—A diagram of the different mechanisms affecting the population of SBS-resonant anti-Stokes phonons Ω_B is shown in Fig. 2(a). In this type of scattering, phonons are annihilated. Therefore, the interaction can be understood as a loss mechanism, present only while the system is optically pumped. The other two processes that affect the phonon occupation are thermal heating and acoustic dissipation. The population of a phonon mode (n_{th}) at a given frequency (Ω) is given by the Bose-Einstein statistics $n_{\mathrm{th}}(\Omega) = 1/(e^{\hbar\Omega/k_B T} - 1)$ and will depend on the temperature of the system (T). As the system thermalizes, the phonon levels are filled with incoherent phonons. Acoustic dissipation, on the other hand, describes the decay of the traveling density fluctuation. While a SBS interaction takes place, energy is being transferred from the acoustic into the optical field, with a coupling strength g_{om}. This results in an effective temperature decrease of the resonant phonon mode.

The shape of the SBS resonances is described by the Lorentzian Brillouin gain spectrum $G_B(\omega) = g_B(\Gamma_{\mathrm{eff}}/2)^2/[(\Omega_B - \omega)^2 + (\Gamma_{\mathrm{eff}}/2)^2]$ where g_B is the intrinsic nonlinear gain of the sample and the effective dissipation rate (Γ_{eff}) is given by the full width at half maximum (FWHM). The effective dissipation rate is defined as $\Gamma_{\mathrm{eff}} = \Gamma_m + \Gamma_{\mathrm{opt}}$, where Γ_m is the natural acoustic dissipation rate and Γ_{opt} is the optically induced loss resulting from the SBS interaction. The cooling rate (R) is defined as the ratio between final and initial phonon occupation, $\bar{n}_f$ and $\bar{n}_0$ respectively. In the weak coupling regime R is given by

$$R = \frac{\bar{n}_f}{\bar{n}_0} = \frac{\Gamma_m}{\Gamma_{\mathrm{eff}}}. \tag{1}$$

From the final phonon population, the effective temperature of the mode after the active cooling can be obtained using the Bose-Einstein equation. In Fig. 2(b) the experimental results for the tapered chalcogenide PCF are shown. From an initial phonon population of 830 at 293 K, a final population of 212 phonons is measured. This corresponds to an effective temperature of 74 K, resulting in a decrease of 219 K or 74.7% from room temperature. Most of the

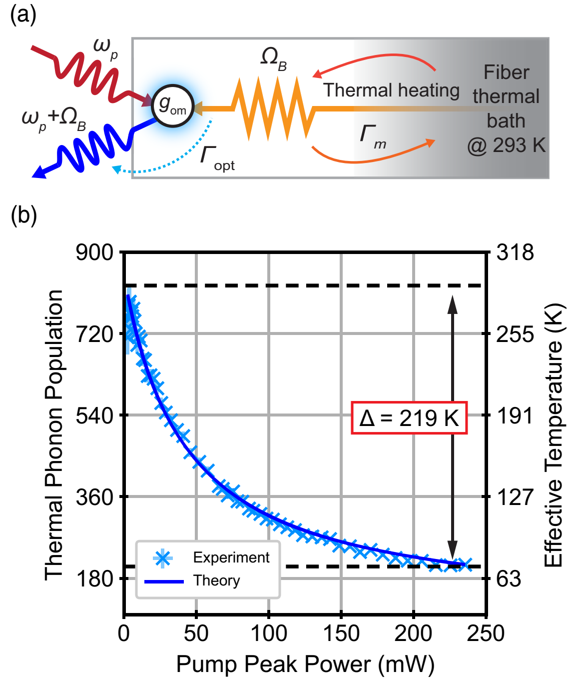

FIG. 2. (a) Diagram of the different processes affecting the population of resonant anti-Stokes phonons at Ω_B. (b) Light blue crosses show the experimentally measured decrease of resonant anti-Stokes phonon population ($\Omega_B/2\pi = 7.38$ GHz) and its respective effective temperature as a function of pump power. From an initial population at room temperature (293 K) of 830 phonons, a final population of 212 is measured, corresponding to 74 K. This results in a temperature decrease of 219 K, or 74.7%. The solid blue line shows the theoretical decrease of phonon population according to Eq. (4). The horizontal black dashed lines are added as visual aids and indicate the initial and final temperature of the phonon mode.

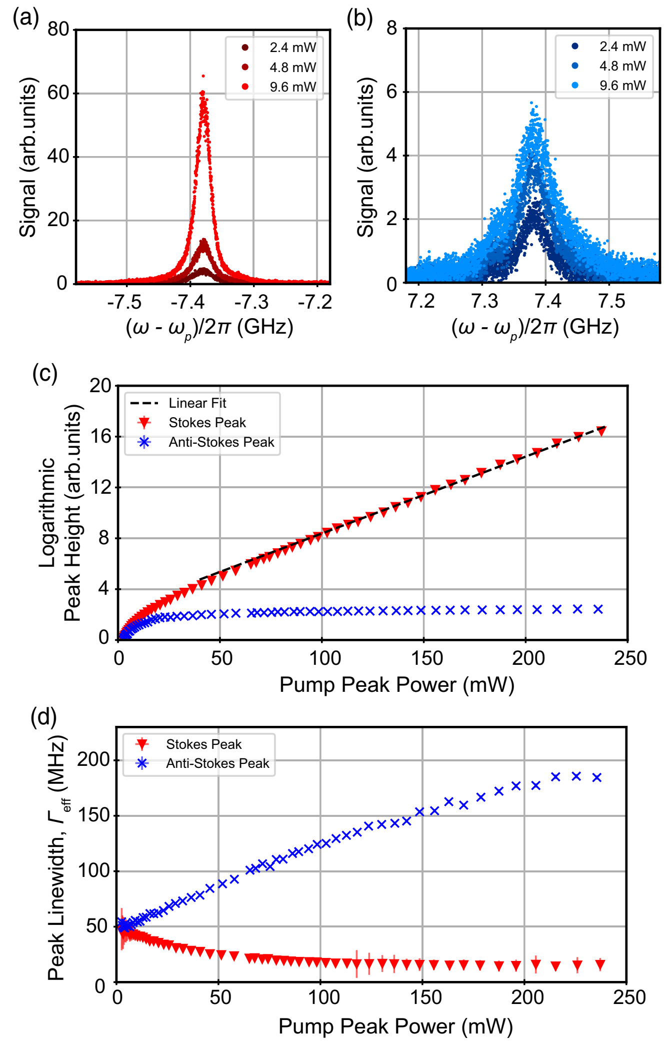

FIG. 3. (a) In red, behavior of the Stokes resonance for three different pump powers. (b) In blue, anti-Stokes resonance for the same powers as (a). Note the different y-axis scales. (c) Peak height of the Stokes (red triangles) and anti-Stokes (blue crosses) resonances in logarithmic scale as a function of pump power. (d) Peak linewidth (Γ_{eff}) of the Stokes (red triangles) and anti-Stokes (blue crosses) resonances as a function of pump power. The Stokes resonance narrows, but the anti-Stokes peaks broadens. This indicates an increase of the effective dissipation rate ($\Gamma_{\mathrm{eff}} = \Gamma_m + \Gamma_{\mathrm{opt}}$) of the addressed phonons, caused by the SBS interaction and a relaxation of the phase-matching condition.

SBS response from the sample comes from the waist of the taper, which is 50 cm long. The phonons addressed in the nonlinear interaction extend all over the active part, resulting thus in a phonon of macroscopic mass being cooled down to cryogenic temperatures. In an optomechanical resonator, both the Stokes and anti-Stokes processes address the same phonon field. For backward SBS in a waveguide system, such as an optical fiber, this symmetry is broken. The resonant longitudinal phonons involved in a Stokes process are copropagating with the pump, while for the anti-Stokes process, they are counterpropagating. Therefore, even if the Stokes scattering is a much more efficient process and the total energy in the acoustic field in the fiber increases, the anti-Stokes resonant phonons are decoupled from it and consequently, the anti-Stokes process is independent. This inherent symmetry breaking allows one to perform the cooling shown without working in the resolved sideband regime. Additionally, both resonances can be studied simultaneously, allowing one to compare their different behaviors [Figs. 3(a) and 3(b)]. The SBS peaks, with a Lorentzian shape, are defined by two parameters, height and linewidth (Γ_{eff}).

The evolution of the peak height as a function of pump power is shown in Fig. 3(c). For low pump powers, both resonances increase in a parallel way, as the initial equilibrium population of the addressed phonon baths are almost equal. After a threshold of 15 mW, the Stokes peak increases exponentially. This behavior is characteristic of stimulated scattering, in which the interference between pump and scattered light and the acoustic waves drive each other, creating a feedback loop. The linear fit of the exponential increase provides the SBS gain of the sample, $g_B = (1.32 \pm 0.18) \times 10^{-9}$ m/W, comparable with literature values [48,49]. The anti-Stokes peak, on the contrary, saturates in height after this threshold. Regarding the linewidths, different behaviors are observed [Fig. 3(d)]. The Stokes resonance narrows, as expected for SBS, while the anti-Stokes broadens. Both the broadening and saturation are footprints of the cooling of phonons via SBS. In the case of a Stokes interaction, the energy is transferred from the optical to the acoustic field, and the amount of phonons that can be created is limited by pump depletion or the damage threshold of the sample. Therefore, an increase in peak height is observed. This is not the case for the anti-Stokes resonance. The number of scattered photons depends on the available number of phonons, fixed by the initial temperature of the thermal bath. As the pump power is increased, more phonons are actively removed from the system, but a limit will be reached. In the ideal case, an observation of peak height saturation would mean that the system has entered a new equilibrium state, in which the thermal bath replenishes the mode at the same speed at which the phonons are actively annihilated. In our experiment this is not the case, as pump depletion arising from the strong Stokes interaction was observed to limit the cooling power [50–54]. The linewidth broadening describes how broad the resonance condition is, i.e., how far from perfect phase-matching the process can still occur. As the pump is increased, more perfectly phase-matched phonons are removed, yet more photons are present. The probability of scattering with an off-resonance phonon therefore broadens.

Theory of Brillouin cooling in waveguides.—An analysis using the theory of waveguide Brillouin optomechanics [44,55,56] of the experimental results is presented in this section. In a typical SBS-active waveguide, backward SBS describes an optoacoustic interaction where two light fields are coherently coupled to an acoustic field. By absorbing a pump photon, the frequency of the backward-scattered photons can be upshifted or downshifted, which corresponds to the Stokes and anti-Stokes processes, respectively. The Stokes process is a parametric down-conversion interaction. It causes heating for acoustic phonons and enables the generation of entangled photon-phonon pairs. The anti-Stokes process is a beam-splitter interaction between scattered photons and acoustic phonons. It can produce phonon cooling, i.e., broadening of the acoustic linewidth, as shown in Figs. 3(b) and 3(d). In addition, the natural dispersive symmetry breaking between the Stokes and anti-Stokes processes in the backward SBS scattering in waveguides allows one to study the anti-Stokes process individually. By giving the system Hamiltonian derived previously in [57,58] and considering the undepleted pump approximation [47], the dynamics of the linearized optoacoustic anti-Stokes interaction in the momentum space can be given by [50]

$$\frac{da_{\mathrm{as}}}{dt} = \left[-i(-\Delta_L + \Delta_1) - \frac{\gamma_o}{2}\right] a_{\mathrm{as}} - i g_{\mathrm{om}} b_{\mathrm{ac}} + \sqrt{\gamma_o}\xi_{\mathrm{as}},$$
$$\frac{db_{\mathrm{ac}}}{dt} = \left[-i(\Omega_B + \Delta_2) - \frac{\Gamma_m}{2}\right] b_{\mathrm{ac}} - i g_{\mathrm{om}} a_{\mathrm{as}} + \sqrt{\Gamma_m}\xi_{\mathrm{ac}}, \qquad (2)$$

where a_{as} (b_{ac}) denote the photon (phonon) annihilation operator for the kth anti-Stokes mode (acoustic mode) with wave number k. Δ_L is the frequency detuning between pump and anti-Stokes fields. γ_o and g_{om} correspond to the optical loss rate and the pump-enhanced optoacoustic coupling strength between anti-Stokes photons and acoustic phonons. $\Delta_1 = k v_{\mathrm{as}}$ and $\Delta_2 = k v_{\mathrm{ac}}$ represent wave-number-induced frequency shifts for the anti-Stokes photons and acoustic phonons, where v_{as} (v_{ac}) is the group velocity of the anti-Stokes (acoustic) wave. ξ_{as} denotes the quantum zero-mean Gaussian noise of the anti-Stokes mode and ξ_{ac} corresponds to the acoustic thermal noise which obeys relations $\langle \xi_{\mathrm{ac}}(t)\rangle = 0$ and $\langle \xi^{\dagger}_{\mathrm{ac}}(t_1)\xi_{\mathrm{ac}}(t_2)\rangle = n_{\mathrm{th}}\delta(t_1 - t_2)$, where n_{th} is the thermal phonon occupation under the environment temperature.

For simplicity, only the case where the anti-Stokes mode and acoustic mode are phase-matched with pump mode, i.e., $\Delta_1 = \Delta_2 = 0$ and $\Delta_L = -\Omega_B$, is discussed. By switching to a frame rotating with frequency Ω_B and considering relations of Langevin noises $\xi_{\mathrm{as,ac}}$, the dynamics of the mean phonon number and photon number can be given by [43]

$$\dot{N}_a = -\gamma_o N_a - i g_{\mathrm{om}}(\langle a^{\dagger}_{\mathrm{as}} b_{\mathrm{ac}}\rangle - \langle a^{\dagger}_{\mathrm{as}} b_{\mathrm{ac}}\rangle^*),$$
$$\dot{N}_b = -\Gamma_m N_b + i g_{\mathrm{om}}(\langle a^{\dagger}_{\mathrm{as}} b_{\mathrm{ac}}\rangle - \langle a^{\dagger}_{\mathrm{as}} b_{\mathrm{ac}}\rangle^*) + \Gamma_m n_{\mathrm{th}},$$
$$\dot{\langle a^{\dagger}_{\mathrm{as}} b_{\mathrm{ac}}\rangle} = -\frac{\gamma_o + \Gamma_m}{2}\langle a^{\dagger}_{\mathrm{as}} b_{\mathrm{ac}}\rangle - i g_{\mathrm{om}} N_a + i g_{\mathrm{om}} N_b, \qquad (3)$$

where $N_a = \langle a^{\dagger}_{\mathrm{as}} a_{\mathrm{as}}\rangle$ and $N_b = \langle b^{\dagger}_{\mathrm{ac}} b_{\mathrm{ac}}\rangle$ correspond to the mean photon and phonon numbers, respectively. Equation (3) can be solved to obtain the phonon occupation at the steady state [50]

$$N_b^{\mathrm{ss}} = \frac{4g^2_{\mathrm{om}} + \gamma_o(\gamma_o + \Gamma_m)}{4g^2_{\mathrm{om}} + \gamma_o\Gamma_m} \cdot \frac{\Gamma_m}{\gamma_o + \Gamma_m} n_{\mathrm{th}}. \qquad (4)$$

From Eq. (4), the cooling rate can be enhanced by increasing the coupling strength g_{om}, i.e., increasing the pump power, as shown in Fig. 2(b). However, this cooling rate will be limited by the ratio $\Gamma_m/(\gamma_o + \Gamma_m)$, similar to the case of sideband cooling in cavity optomechanics [59–61]. The optically enhanced acoustic damping rate is defined thus as

$$\Gamma_{\mathrm{eff}} = \Gamma_m + \frac{4g^2_{\mathrm{om}}\gamma_o}{4g^2_{\mathrm{om}} + \gamma_o(\Gamma_m + \gamma_o)}, \qquad (5)$$

which can be seen in Figs. 3(b) and 3(d), as the anti-Stokes resonance broadens with increasing input power. Equation (5) shows a saturation in linewidth for high pump powers, indicating a physical limit for the phonon cooling achievable through this process. Given the system parameters in this experiment, the minimum phonon population achievable from room temperature is around 100 phonons, corresponding to an effective temperature of 36 K ($R = 0.1$). It should be noted that this system is a continuous optomechanical system, which provides cooling for groups of phonons [43,46], instead of single-mode or multimode mechanical cooling in cavity optomechanical systems. In Eq. (3), only the phase-matching case with zero wave number is considered. For acoustic modes with nonzero wave number, the cooling rate at a steady state can be calculated by including the effects of the wave-number-induced frequency shifts $\Delta_{1,2}$ [50].

Conclusions and outlook.—This experiment has demonstrated that SBS is a promising tool in the challenge of bringing waveguide modes to their quantum ground state of mechanical motion. A massive 50 cm long phonon with frequency 7.38 GHz is brought to cryogenic temperatures from room temperature, reducing the effective mode temperature by 219 K, one order of magnitude higher than previously reported [46]. This improvement is due to the higher pump power used and the choice of experimental platform, a tapered solid core chalcogenide glass PCF, that enables efficient coupling of optical and acoustic waves and has better power handling capabilities. The high gain material [48,49] and microstructure [62,63], combined with the longer interaction lengths achievable in a fiber, allow one to perform cooling to such a strong degree. The material is moreover not limited by two-photon absorption and nonlinear optical loss, as silicon platforms are [46]. With our novel theoretical description of the cooling process, the physical cooling limit was calculated to be 90% of population decrease. This opens the path to the realistic achievement of reaching the quantum ground state in waveguides, given the high frequency of the resonant phonons addressed in this experiment. Performing the experiment in a cryogenic environment, such as a liquid helium cryostat at 4 K, paired with the efficient cooling present in the fiber, would produce occupations of few or even less than one phonon. This is a crucial prerequisite for observing quantum phenomena in macroscopic optoacoustic systems, such as the generation of entangled photon-phonon pairs and quantum state transfer between optical photons and acoustic phonons. Consequently, it would enable new quantum technologies, including quantum storage and repeater schemes [44]. These results therefore pave the way toward accessing the quantum nature of massive objects. A similar work was published [64] showing cooling by 21 K in a liquid-core fiber.

We thank C. Silberhorn and C. Wolff and our co-workers A. Popp, X. Zeng, S. Becker, Z. O. Saffer, and J. Landgraf for valuable discussions. We acknowledge funding from the Max Planck Society through the Independent Max Planck Research Group scheme.

[*]Contributed equally to this work.
[†]Corresponding author: birgit.stiller@mpl.mpg.de

[1] A. D. O'Connell, M. Hofheinz, M. Ansmann, R. C. Bialczak, M. Lenander, E. Lucero, M. Neeley, D. Sank, H. Wang, M. Weides, J. Wenner, J. M. Martinis, and A. N. Cleland, Quantum ground state and single-phonon control of a mechanical resonator, Nature (London) **464**, 697 (2010).

[2] J. D. Teufel, T. Donner, D. Li, J. W. Harlow, M. S. Allman, K. Cicak, A. J. Sirois, J. D. Whittaker, K. W. Lehnert, and R. W. Simmonds, Sideband cooling of micromechanical motion to the quantum ground state, Nature (London) **475**, 359 (2011).

[3] J. Chan, T. P. M. Alegre, A. H. Safavi-Naeini, J. T. Hill, A. Krause, S. Gröblacher, M. Aspelmeyer, and O. Painter, Laser cooling of a nanomechanical oscillator into its quantum ground state, Nature (London) **478**, 89 (2011).

[4] U. Delić, M. Reisenbauer, K. Dare, D. Grass, V. Vuletić, N. Kiesel, and M. Aspelmeyer, Cooling of a levitated nanoparticle to the motional quantum ground state, Science **367**, 892 (2020).

[5] H. M. Doeleman, T. Schatteburg, R. Benevides, S. Vollenweider, D. Macri, and Y. Chu, Brillouin optomechanics in the quantum ground state, Phys. Rev. Res. **5**, 043140 (2023).

[6] I. Wilson-Rae, P. Zoller, and A. Imamoğlu, Laser cooling of a nanomechanical resonator mode to its quantum ground state, Phys. Rev. Lett. **92**, 075507 (2004).

[7] F. Xue, Y. D. Wang, C. P. Sun, H. Okamoto, H. Yamaguchi, and K. Semba, Controllable coupling between flux qubit and nanomechanical resonator by magnetic field, New J. Phys. **9**, 35 (2007).

[8] D. Kleckner and D. Bouwmeester, Sub-kelvin optical cooling of a micromechanical resonator, Nature (London) **444**, 75 (2006).

[9] O. Arcizet, P.-F. Cohadon, T. Briant, M. Pinard, A. Heidmann, J.-M. Mackowski, C. Michel, L. Pinard, O. Français, and L. Rousseau, High-sensitivity optical monitoring of a micromechanical resonator with a quantum-limited optomechanical sensor, Phys. Rev. Lett. **97**, 133601 (2006).

[10] J. Guo, R. Norte, and S. Gröblacher, Feedback cooling of a room temperature mechanical oscillator close to its motional ground state, Phys. Rev. Lett. **123**, 223602 (2019).

[11] D. Su, Y. Jiang, P. Solano, L. A. Orozco, J. Lawall, and Y. Zhao, Optomechanical feedback cooling of a 5 mm-long torsional mode, Photonics Res. **11**, 2179 (2023).

[12] J. B. Clark, F. Lecocq, R. W. Simmonds, J. Aumentado, and J. D. Teufel, Sideband cooling beyond the quantum back-action limit with squeezed light, Nature (London) **541**, 191 (2017).

[13] A. Schliesser, P. Del'Haye, N. Nooshi, K. J. Vahala, and T. J. Kippenberg, Radiation pressure cooling of a micromechanical oscillator using dynamical backaction, Phys. Rev. Lett. **97**, 243905 (2006).

[14] F. Marquardt, J. P. Chen, A. A. Clerk, and S. M. Girvin, Quantum theory of cavity-assisted sideband cooling of mechanical motion, Phys. Rev. Lett. **99**, 093902 (2007).

[15] I. Wilson-Rae, N. Nooshi, W. Zwerger, and T. J. Kippenberg, Theory of ground state cooling of a mechanical oscillator using dynamical backaction, Phys. Rev. Lett. **99**, 093901 (2007).

[16] I. Favero and K. Karrai, Optomechanics of deformable optical cavities, Nat. Photonics **3**, 201 (2009).

[17] S. Gigan, H. R. Böhm, M. Paternostro, F. Blaser, G. Langer, J. B. Hertzberg, K. C. Schwab, D. Bäuerle, M. Aspelmeyer, and A. Zeilinger, Self-cooling of a micromirror by radiation pressure, Nature (London) **444**, 67 (2006).

[18] C. A. Regal, J. D. Teufel, and K. W. Lehnert, Measuring nanomechanical motion with a microwave cavity interferometer, Nat. Phys. **4**, 555 (2008).

[19] C. M. Caves, K. S. Thorne, R. W. P. Drever, V. D. Sandberg, and M. Zimmermann, On the measurement of a weak classical force coupled to a quantum-mechanical oscillator. I. Issues of principle, Rev. Mod. Phys. **52**, 341 (1980).

[20] S. Jevtic, D. Newman, T. Rudolph, and T. M. Stace, Single-qubit thermometry, Phys. Rev. A **91**, 012331 (2015).

[21] L. A. Correa, M. Mehboudi, G. Adesso, and A. Sanpera, Individual quantum probes for optimal thermometry, Phys. Rev. Lett. **114**, 220405 (2015).

[22] S. Bose, K. Jacobs, and P. L. Knight, Preparation of nonclassical states in cavities with a moving mirror, Phys. Rev. A **56**, 4175 (1997).

[23] K. Jähne, C. Genes, K. Hammerer, M. Wallquist, E. S. Polzik, and P. Zoller, Cavity-assisted squeezing of a mechanical oscillator, Phys. Rev. A **79**, 063819 (2009).

[24] K. Jaehne, K. Hammerer, and M. Wallquist, Ground-state cooling of a nanomechanical resonator via a Cooper-pair box qubit, New J. Phys. **10**, 095019 (2008).

[25] W. Marshall, C. Simon, R. Penrose, and D. Bouwmeester, Towards quantum superpositions of a mirror, Phys. Rev. Lett. **91**, 130401 (2003).

[26] C. Whittle, A. Pele, R. M. S. Schofield, D. Sigg, M. Tse, G. Vajente, D. C. Vander-Hyde, H. Yu *et al.*, Approaching the motional ground state of a 10-kg object, Science **372**, 1333 (2021).

[27] C. Wolff, M. J. A. Smith, B. Stiller, and C. G. Poulton, Brillouin scattering—theory and experiment: Tutorial, J. Opt. Soc. Am. B **38**, 1243 (2021).

[28] M. Niklès, L. Thévenaz, and P. A. Robert, Simple distributed fiber sensor based on Brillouin gain spectrum analysis, Opt. Lett. **21**, 758 (1996).

[29] A. Geilen, A. Popp, D. Das, S. Junaid, C. G. Poulton, M. Chemnitz, C. Marquardt, M. A. Schmidt, and B. Stiller, Extreme thermodynamics in nanolitre volumes through stimulated Brillouin-Mandelstam scattering, Nat. Phys. **19**, 1805 (2023).

[30] K. Hotate and T. Hasegawa, Measurement of Brillouin gain spectrum distribution along an optical fiber using a correlation-based technique: Proposal, experiment and simulation, IEICE Trans. Electron. **E83-C**, 405 (2000).

[31] B. Vidal, M. A. Piqueras, and J. Martí, Tunable and reconfigurable photonic microwave filter based on stimulated Brillouin scattering, Opt. Lett. **32**, 23 (2007).

[32] Y. Liu, A. Choudhary, D. Marpaung, and B. J. Eggleton, Integrated microwave photonic filters, Adv. Opt. Photonics **12**, 485 (2020).

[33] X. Zeng, P. S. Russell, C. Wolff, M. H. Frosz, G. K. L. Wong, and B. Stiller, Nonreciprocal vortex isolator via topology-selective stimulated Brillouin scattering, Sci. Adv. **8**, eabq6064 (2022).

[34] M. Merklein, B. Stiller, K. Vu, S. J. Madden, and B. J. Eggleton, A chip-integrated coherent photonic-phononic memory, Nat. Commun. **8**, 574 (2017).

[35] Z. Zhu, D. J. Gauthier, and R. W. Boyd, Stored light in an optical fiber via stimulated Brillouin scattering, Science **318**, 1748 (2007).

[36] B. Stiller, M. Merklein, C. Wolff, K. Vu, P. Ma, S. J. Madden, and B. J. Eggleton, Coherently refreshing hypersonic phonons for light storage, Optica **7**, 492 (2020).

[37] D. Marpaung, M. Pagani, B. Morrison, and B. J. Eggleton, Nonlinear integrated microwave photonics, J. Lightwave Technol. **32**, 3421 (2014).

[38] D. Marpaung, J. Yao, and J. Capmany, Integrated microwave photonics, Nat. Photonics **13**, 80 (2019).

[39] M. Merklein, A. Casas-Bedoya, D. Marpaung, T. F. S. Büttner, M. Pagani, B. Morrison, I. V. Kabakova, and B. J. Eggleton, Stimulated Brillouin scattering in photonic integrated circuits: Novel applications and devices, IEEE J. Sel. Top. Quantum Electron. **22**, 336 (2016).

[40] K. O. Hill, D. C. Johnson, and B. S. Kawasaki, CW generation of multiple Stokes and anti-Stokes Brillouin-shifted frequencies, Appl. Phys. Lett. **29**, 185 (1976).

[41] N. T. Otterstrom, R. O. Behunin, E. A. Kittlaus, Z. Wang, and P. T. Rakich, A silicon Brillouin laser, Science **360**, 1113 (2018).

[42] X. Zeng, P. S. J. Russell, Y. Chen, Z. Wang, G. K. L. Wong, P. Roth, M. H. Frosz, and B. Stiller, Optical vortex Brillouin laser, Laser Photonics Rev. **17**, 2200277 (2023).

[43] C. Zhu and B. Stiller, Dynamic Brillouin cooling for continuous optomechanical systems, Mater. Quantum Technol. **3**, 015003 (2023).

[44] J. Zhang, C. Zhu, C. Wolff, and B. Stiller, Quantum coherent control in pulsed waveguide optomechanics, Phys. Rev. Res. **5**, 013010 (2023).

[45] G. Bahl, M. Tomes, F. Marquardt, and T. Carmon, Observation of spontaneous Brillouin cooling, Nat. Phys. **8**, 203 (2012).

[46] N. T. Otterstrom, R. O. Behunin, E. A. Kittlaus, and P. T. Rakich, Optomechanical cooling in a continuous system, Phys. Rev. X **8**, 041034 (2018).

[47] Y. C. Chen, S. Kim, and G. Bahl, Brillouin cooling in a linear waveguide, New J. Phys. **18**, 115004 (2016).

[48] K. S. Abedin, Observation of strong stimulated Brillouin scattering in single-mode As_2Se_3 chalcogenide fiber, Opt. Express **13**, 10266 (2005).

[49] K. Ogusu, H. Li, and M. Kitao, Brillouin-gain coefficients of chalcogenide glasses, J. Opt. Soc. Am. B **21**, 1302 (2004).

[50] See Supplemental Material, which includes Refs. [51-54], at http://link.aps.org/supplemental/10.1103/PhysRevLett.132.023603 for additional derivations of the equation of linearized SBS interaction, analysis of Brillouin-Mandelstam cooling via the covariance approach, and an experimental study of the pump depletion via the Stokes wave limiting cooling.

[51] P. Kharel, R. O. Behunin, W. H. Renninger, and P. T. Rakich, Noise and dynamics in forward Brillouin interactions, Phys. Rev. A **93**, 063806 (2016).

[52] Y.-C. Liu, Y.-W. Hu, C. W. Wong, and Y.-F. Xiao, Review of cavity optomechanical cooling, Chin. Phys. B **22**, 114213 (2013).

[53] R. W. Boyd, *Nonlinear Optics* (Academic Press, New York, 2020).

[54] E. Ippen and R. Stolen, Stimulated Brillouin scattering in optical fibers, Appl. Phys. Lett. **21**, 539 (1972).

[55] R. Van Laer, R. Baets, and D. Van Thourhout, Unifying Brillouin scattering and cavity optomechanics, Phys. Rev. A **93**, 053828 (2016).

[56] P. Rakich and F. Marquardt, Quantum theory of continuum optomechanics, New J. Phys. **20**, 045005 (2018).

[57] J. E. Sipe and M. J. Steel, A Hamiltonian treatment of stimulated Brillouin scattering in nanoscale integrated waveguides, New J. Phys. **18**, 045004 (2016).

[58] H. Zoubi and K. Hammerer, Optomechanical multimode Hamiltonian for nanophotonic waveguides, Phys. Rev. A **94**, 053827 (2016).

[59] M. Aspelmeyer, T. J. Kippenberg, and F. Marquardt, Cavity optomechanics, Rev. Mod. Phys. **86**, 1391 (2014).

[60] C. Genes, D. Vitali, P. Tombesi, S. Gigan, and M. Aspelmeyer, Ground-state cooling of a micromechanical oscillator: Comparing cold damping and cavity-assisted cooling schemes, Phys. Rev. A **77**, 033804 (2008).

[61] L. Qiu, I. Shomroni, P. Seidler, and T. J. Kippenberg, Laser cooling of a nanomechanical oscillator to its zero-point energy, Phys. Rev. Lett. **124**, 173601 (2020).

[62] L. Brilland, P. Houizot, J. Troles, F. Désévédavy, Q. Coulombier, J. Fatome, C. Fortier, F. Smektala, K. Messadd, B. Kibler, S. Pitois, G. Gadret, C. Finot, T. Nguyen, T. Chartier, M. Thual, G. Renversez, N. Traynor, and J. L. Adam, Recent progress on the realization of chalcogenides photonic crystal fibers, in *Optical Components and Materials VI* (SPIE, 2009), Vol. 7212, pp. 115–126.

[63] S. Gao and X. Bao, Chalcogenide taper and its nonlinear effects and sensing applications, iScience **23**, 100802 (2020).

[64] J. N. Johnson, D. R. Haverkamp, Y.-H. Ou, K. Kieu, N. T. Otterstrom, P. T. Rakich, and R. O. Behunin, Laser cooling of traveling wave phonons in an optical fiber, arXiv:2305.11796.